analytical chemistry

Letter

pubs.acs.org/ac

Liposome-Coated Persistent Luminescence Nanoparticles as Luminescence Trackable Drug Carrier for Chemotherapy

Li-Jian Chen,[†] Cheng-Xiong Yang,[†] and Xiu-Ping Yan*[,†,‡]

[†]College of Chemistry, Research Center for Analytical Sciences, State Key Laboratory of Medicinal Chemical Biology, Tianjin Key Laboratory of Molecular Recognition and Biosensing, Nankai University, 94 Weijin Road, Tianjin 300071, China

[‡]Collaborative Innovation Center of Chemical Science and Engineering (Tianjin), 94 Weijin Road, Tianjin 300071, China

Supporting Information

ABSTRACT: Near-infrared persistent luminescence nanoparticles (NIR-PLNPs) are promising imaging agents due to deep tissue penetration, high signal-to-noise ratio, and repeatedly charging ability. Here, we report liposome-coated NIR-PLNPs (Lipo-PLNPs) as a novel persistent luminescence imaging guided drug carrier for chemotherapy. The Lipo-PLNP nanocomposite shows the advantages of superior persistent luminescence and high drug loading efficiency and enables autofluorescence-free and long-term tracking of drug delivery carriers with remarkable therapeutic effect.

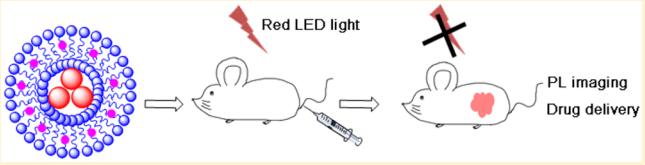

Nanotechnology has produced a great impact on cancer diagnosis and therapy applications.[1,2] The afterglow of persistent luminescence nanoparticles (PLNPs) can last for hours or even days after stopping the external excitation. Compared with traditional fluorescent imaging materials, PLNPs successfully avoids strong tissue autofluorescence, phototoxicity, and photobleaching in bioimaging.[3,4] In particular, near-infrared (NIR) emitting PLNPs have emerged as promising in vivo optical imaging agents due to the advantages of deep tissue penetration, and no in situ excitation is needed.[5−8] Therefore, PLNPs have been considered as a new generation of superior bioimaging contrast agents due to high signal-to-noise ratio (SNR). Moreover, Cr^{3+}-doped NIR-emitting PLNPs can be reactivated under a tissue-penetrating red light-emitting diode (LED); thus, their application to in vivo imaging is no longer limited by afterglow time.[7,9]

Engineering PLNPs to multifunctional nanocomposites for simultaneous bioimaging and therapy is a recent hot research topic.[10,11] Such examples include multifunctional PLNP/CuS nanoprobe for in vivo activatable luminescence imaging and effective photothermal therapy[12] and indocyanine green and PLNP coloaded mesoporous silica nanocarriers for persistent luminescence imaging and photothermal therapy.[13] Usually, mesoporous silica nanoparticles are integrated into PLNP as trackable drug carriers due to the mesoporous structure and large specific surface area.[14,15] However, synthesis of mesoporous silica-based nanocomposites is relatively complicated and time-consuming. In particular, the loading efficiency is relatively low, and complex modification is needed when hydrophobic drugs are encapsulated,[16,17] which greatly limits their application as drug carriers.

Liposomes are spherical-shaped nanovehicles consisting of concentric lipid bilayer entrapping an internal aqueous core.[18] They are extensively approved for biomedical applications with merits of biocompatibility, biodegradability, and low toxicity.[19,20] Especially, liposomes have been applied as the carriers of hydrophobic[17,21] and hydrophilic drugs,[18] gene agents,[22] and anticancer metals[23] as well as imaging contrast agents.[24,25] However, it is hard to monitor in real-time drug encapsulated liposomes in biological systems due to the absence of detectable signals. Therefore, it is necessary to develop nanoplatforms to integrate imaging agents and drug carriers for in vivo monitoring the delivery route of drug carriers.

Herein, we report the preparation and application of liposome-coated PLNPs (Lipo-PLNPs) as the carrier of paclitaxel (PTX) for luminescence imaging guided chemotherapy. PTX, which is a water insoluble antitumor drug of wide spectrum and hard to modify, can be successfully encapsulated in liposomes and improve therapeutic efficiency.[26−28] $Zn_{1.1}Ga_{1.8}Ge_{0.1}O_4:Cr^{3+}$ PLNP is used as imaging contrast agent due to the long persistent luminescence and red LED light-renewable ability.[12] Lipo-PLNPs are simply prepared using a thin layer evaporation method. The developed Lipo-PLNPs not only show high drug loading efficiency but also possess superior bioimaging ability without autofluorescence in vivo. Furthermore, Lipo-PLNPs can passively target the human breast cancer (MCF-7) xenograft in nude mice with enhanced permeability and retention (EPR) effect, acquiring effective cancer therapy.

RESULTS AND DISCUSSION

Well-dispersed $Zn_{1.1}Ga_{1.8}Ge_{0.1}O_4:Cr^{3+}$ PLNP was synthesized using a direct hydrothermal method without high-temperature sintering.[9,12] The PLNP shows an average size of 27.6 ± 4.6 nm

Received: April 13, 2017
Accepted: June 13, 2017
Published: June 13, 2017

DOI: 10.1021/acs.analchem.7b01397
Anal. Chem. 2017, 89, 6936−6939

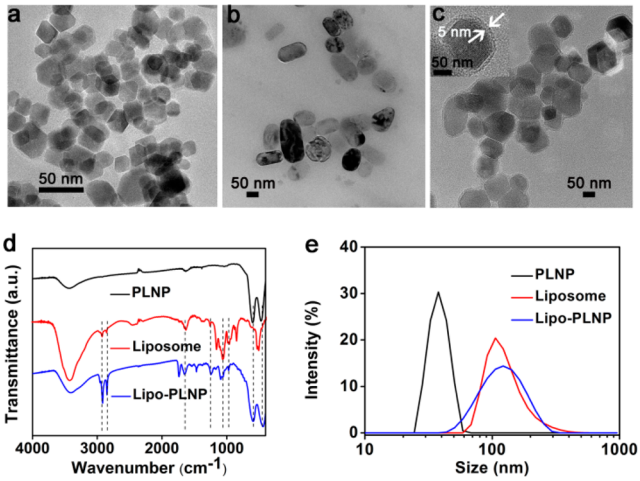

Figure 1. (a) Transmission electron microscopy (TEM) image of the PLNP. (b) TEM image of the liposomes. (c) TEM image of the Lipo-PLNPs. (d) FT-IR spectra of the PLNP, liposomes, and Lipo-PLNP. (e) Hydrodynamic size distribution of the PLNP, liposomes, and Lipo-PLNP.

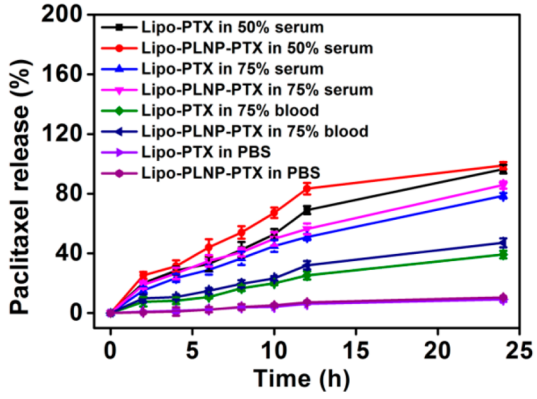

Figure 2. In vitro release properties of the PTX from Lipo-PTX and Lipo-PLNP-PTX in different media at 37 °C (50% human serum, 75% human serum, and 75% human blood, respectively) or under storage conditions (10 mM PBS, pH 7.4, 4 °C).

(Figure 1a) with a cubic spinel structure of Zn_2GeO_4 (JCPDS 25-1018) and $ZnGa_2O_4$ (JCPDS 38-1240) (Figure S1). Liposomes and Lipo-PLNPs were prepared using the thin layer evaporation and subsequent hydration method.[29] The as-prepared liposomes show the morphology of lipid bilayer vesicles with an average size of 100.4 ± 12.8 nm (Figure 1b). The Lipo-PLNP has an average size of 112.5 ± 18.3 nm with a 5 nm-thick lipid layer coating (Figures 1c and S2a,b). The PTX loaded Lipo-PLNP (Lipo-PLNP-PTX) shows an obscure bilayer due to the PTX encapsulation (Figure S4a).

The Lipo-PLNP shows not only the characteristic Fourier transform infrared (FT-IR) vibration bands of PLNP (465 cm^{-1} for Ga−O bending, 610 cm^{-1} for Zn−O bending) but also those of liposomes (2925 and 2853 cm^{-1} for $-CH_2-$ asymmetric and symmetric stretching, respectively; 1737 cm^{-1} for C = O bending; 1268 and 1072 cm^{-1} for P = O asymmetric and symmetric stretching, respectively; 974 cm^{-1} for $N-CH_3$ stretching), confirming the successful preparation of Lipo-PLNP (Figure 1d). Lipo-PLNPs gave much larger hydrodynamic size (122.0 nm) than the PLNP (37.8 nm) (Figure 1e) but much less positive Zeta potential (+6.6 mV) than the

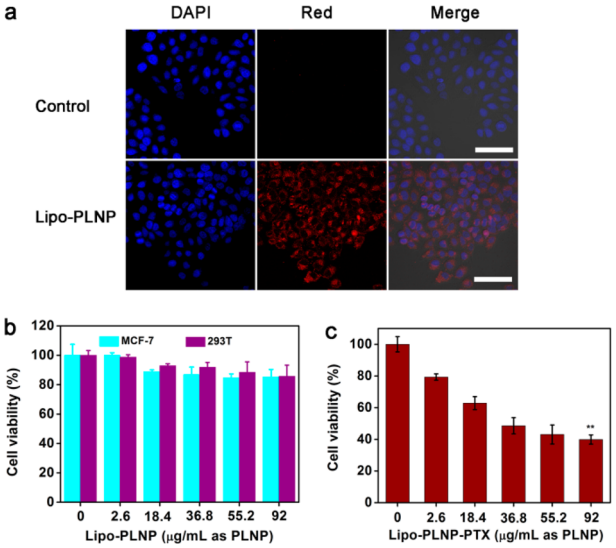

Figure 3. (a) Cellular uptake of Lipo-PLNPs in MCF-7 cells. The red color represents the intracellular location of the Lipo-PLNPs, and the blue color results from DAPI for cell nuclei staining. Scale bar: 100 μm. (b) Cell viability of MCF-7 and 293T cells against different concentrations of Lipo-PLNPs. (c) Cell viability of MCF-7 cells against different concentrations of Lipo-PLNP-PTX. $^{**}P < 0.01$.

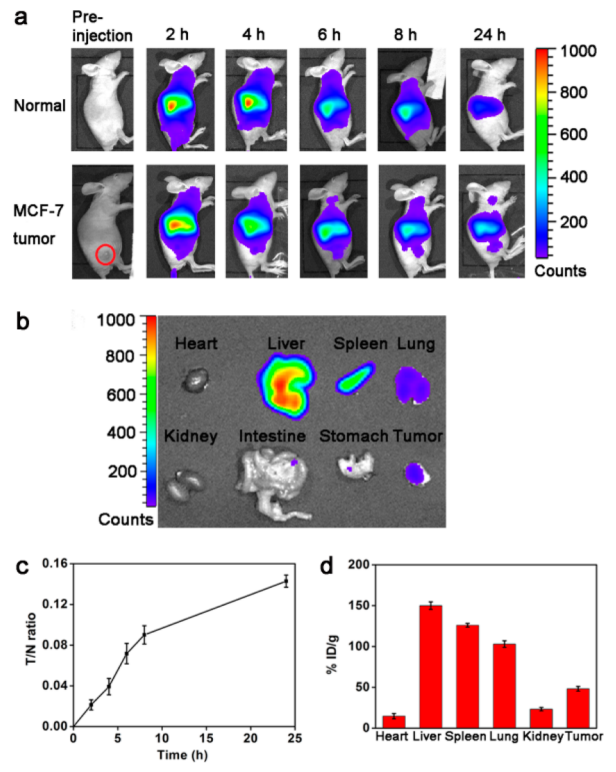

Figure 4. (a) In vivo persistent luminescence images of normal mice and MCF-7 tumor-bearing mice after intravenous injection of Lipo-PLNP-PTX (10 min excitation with a 254 nm UV light before intravenous injection, 2 min excitation with LED lamp before each acquisition). (b) Persistent luminescence images of tumor and major organs dissected from sacrificed tumor-bearing mice at 24 h postinjection. (c) Signal ratio of tumor to normal tissues (T/N) of MCF-7 tumor-bearing mice (n = 3) as a function of time. (d) Biodistribution of Lipo-PLNPs in MCF-7 tumor-bearing mice (n = 3) at 24 h after intravenous injection. % ID/g is the percentage of injected dose per gram.

DOI: 10.1021/acs.analchem.7b01397
Anal. Chem. 2017, 89, 6936−6939

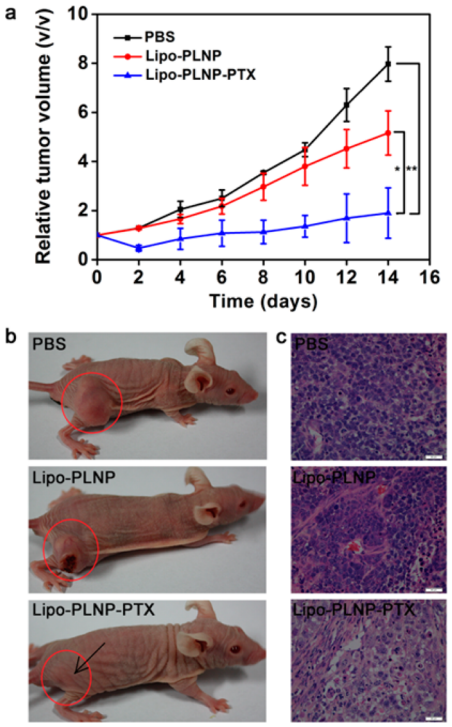

Figure 5. (a) MCF-7 tumor growth curves of three mice groups after various treatments. *P < 0.05, **P < 0.01. (b) Representative photographs of mice from different groups after a 14 day treatment. (c) Histological staining of tumor tissues from different treated mice groups. Scale bar: 20 μm.

PLNP (+27.0 mV) due to the coating of negative liposomes (Figure S2c).

The as-prepared PLNP shows luminescence emission at 695 nm ($^2E \rightarrow {}^4A_2$ transition) and three characteristic excitation bands at 280 nm (band-to-band transition), 440 nm ($^2A_2 \rightarrow {}^4T_1$ transition), and 570 nm ($^2A_2 \rightarrow {}^4T_2$ transition) (Figure S3a).[6,7] The PLNP exhibits good persistent luminescence after 5 min of illumination with a UV lamp due to the slow release of the stored energy after excitation (Figure S3b). Moreover, the persistent luminescence can be repeatedly activated by a red LED light, which is deep tissue penetrating (Figure S3c). The Lipo-PLNP and Lipo-PLNP-PTX still maintains strong emission intensity and long-time persistent luminescence (Figure S4b–d), indicating the potential of Lipo-PLNP and Lipo-PLNP-PTX for in vivo imaging applications.

The Lipo-PLNP-PTX still shows high drug encapsulation efficiency (69.2 ± 2.8%), although less than that of the PTX loaded liposome (Lipo-PTX) (89.2 ± 1.5%). The drug release of the drug carrier Lipo-PLNP-PTX was studied in different media. Human serum and blood were used to mimic the in vivo environment. From Figure 2, the Lipo-PLNP-PTX shows a similar drug release (98.9 ± 2.4%) in 50% human serum at 37 °C after 24 h, compared with that of the Lipo-PTX (96.5 ± 2.9%). The Lipo-PLNP-PTX and Lipo-PTX show a little slower drug release (85.9 ± 2.4%, 78.6 ± 1.9%) in 75% human serum and a much slower drug release (47.1 ± 3.0%, 39.2 ± 2.5%) in 75% blood. However, the Lipo-PLNP-PTX and Lipo-PTX show limited drug release in PBS (10 mM, pH 7.4) at 4 °C after 24 h (10.5 ± 0.3%, 9.1 ± 0.5%, respectively), indicating relatively good stability of the drug carriers under storage conditions.

Human breast cancer (MCF-7) cells were incubated with Lipo-PLNPs to investigate the application of Lipo-PLNPs for imaging cancer cells. Luminescence signal in MCF-7 cells was obviously observed compared to the control group, indicating the successful internalization of Lipo-PLNPs in cancer cells (Figure 3a). The result suggests that the Lipo-PLNPs are capable of imaging cancer cells in vitro. To evaluate the cytotoxicity of Lipo-PLNPs, MCF-7 and 293T cells were treated with different concentrations of Lipo-PLNPs for 24 h. The cell viabilities are still over 85%, showing low cytotoxicity of Lipo-PLNPs (Figure 3b). In addition, the in vitro cytotoxicity of Lipo-PLNP-PTX was also evaluated. The cell viability of MCF-7 cells treated with Lipo-PLNP-PTX decreased to 39.8%, even at the low PTX concentration (2.5 μg/mL, 92 μg mL^{-1} as PLNP) (Figure 3c). These results reveal that Lipo-PLNP-PTX has superior therapeutic efficacy in vitro.

To study the imaging ability of Lipo-PLNPs in vivo, the Lipo-PLNPs were intravenously injected into normal mice. As shown in Figure S6, luminescence signals were observed for at least 7 days after injection. Strong luminescence intensity was observed in liver and spleen, showing the accumulation of Lipo-PLNPs in the reticuloendothelial system organs (RES). These results indicate that Lipo-PLNPs possess the long-term bioimaging ability and can be used as trackable drug carrier in vivo.

To further study the imaging ability of PTX-loaded nanocomposite in vivo, Lipo-PLNP-PTX was intravenously injected into normal mice and MCF-7 tumor-bearing mice, respectively. The luminescence signal was visualized nearly in the whole body at 2 h postinjection, suggesting the distribution of the composite throughout the body (Figure 4a). Compared with the normal mice, luminescence signal was obviously observed in the tumor area of tumor-bearing mice at 4 h and increased at 24 h postinjection (Figure 4c), indicating the composite can be accumulated to the tumor site due to long-time circulation and EPR effect. The ex vivo persistent luminescence images of tumor and main organs showed the most luminescence signals in liver, spleen, lung, and tumor (Figure 4b), which was fairly consistent with the biodistribution result indicated by the Zn concentration (from PLNP) in the organs determined by ICPMS (Figure 4d). The bioimaging of Lipo-PLNPs plays a role in guidance of further therapeutic application.

To investigate the therapeutic efficacy of Lipo-PLNP-PTX in vivo, MCF-7 tumor-bearing athymic mice were randomly divided into three groups (one experimental group treated with Lipo-PLNP-PTX, two control groups treated with Lipo-PLNPs or PBS only). The tumor volume curves and representative photographs of the mice show that tumor growth was dramatically inhibited by Lipo-PLNP-PTX (Figure 5a,b), indicating the effectiveness of PTX for killing cancer cells. The histology study confirms that the Lipo-PLNP-PTX administered by intravenous injection induced significant necrotic response (Figure 5c). These results suggest that Lipo-PLNPs are a kind of promising drug carrier for cancer therapy in vivo.

To further evaluate the toxicity of Lipo-PLNPs in vivo, H&E staining of major organs was performed (Figure S8). No remarkable damage sign of the organs such as liver, spleen, heart, lung, and kidney was found. In addition, the cumulative excretion of the nanoparticles was studied. The result shows that 74.1% of the nanoparticles were excreted via feces of mice in 10 days after intravenous injection (Figure S7). The results

DOI: 10.1021/acs.analchem.7b01397
Anal. Chem. 2017, 89, 6936−6939

demonstrate that Lipo-PLNPs possess minimal toxicity in healthy mice.

In summary, we have reported a novel persistent luminescence imaging guided drug carrier for chemotherapy. The integration of PLNPs and liposomes renders the Lipo-PLNPs high drug loading and therapeutic efficacy with excellent imaging ability without autofluorescence interference, making Lipo-PLNPs promising as trackable drug delivery vehicles for biomedical applications.

■ ASSOCIATED CONTENT

Supporting Information

The Supporting Information is available free of charge on the ACS Publications website at DOI: 10.1021/acs.analchem.7b01397.

Chemicals, characterization, experimental details of Lipo-PLNPs synthesis, methods for PTX analysis and HPLC detection, imaging and therapeutic experiments in vivo and in vitro, and supplemental figures (PDF)

■ AUTHOR INFORMATION

Corresponding Author

*Fax: (86) 22 23506075. E-mail: xpyan@nankai.edu.cn.

ORCID

Li-Jian Chen: 0000-0001-8671-8766

Xiu-Ping Yan: 0000-0001-9953-7681

Notes

The authors declare no competing financial interest.

■ ACKNOWLEDGMENTS

The authors appreciate the support from the National Natural Science Foundation of China (21435001) and Open Funds of the State Key Laboratory of Electroanalytical Chemistry (SKLEAC201705).

■ REFERENCES

(1) Kim, J.; Piao, Y.; Hyeon, T. *Chem. Soc. Rev.* **2009**, *38*, 372−390.

(2) Lee, D. E.; Koo, H.; Sun, I. C.; Ryu, J. H.; Kim, K.; Kwon, I. C. *Chem. Soc. Rev.* **2012**, *41*, 2656−2672.

(3) Chen, G.; Qiu, H.; Prasad, P. N.; Chen, X. *Chem. Rev.* **2014**, *114*, 5161−5214.

(4) Wegner, K. D.; Hildebrandt, N. *Chem. Soc. Rev.* **2015**, *44*, 4792−4834.

(5) le Masne de Chermont, Q.; Chaneac, C.; Seguin, J.; Pelle, F.; Maitrejean, S.; Jolivet, J. P.; Gourier, D.; Bessodes, M.; Scherman, D. *Proc. Natl. Acad. Sci. U. S. A.* **2007**, *104*, 9266−9271.

(6) Abdukayum, A.; Chen, J. T.; Zhao, Q.; Yan, X. P. *J. Am. Chem. Soc.* **2013**, *135*, 14125−14133.

(7) Maldiney, T.; Bessière, A.; Seguin, J.; Teston, E.; Sharma, S. K.; Viana, B.; Bos, A. J. J.; Dorenbos, P.; Bessodes, M.; Gourier, D.; Scherman, D.; Richard, C. *Nat. Mater.* **2014**, *13*, 418−426.

(8) Pan, Z.; Lu, Y.-Y.; Liu, F. *Nat. Mater.* **2012**, *11*, 58−63.

(9) Li, Z.; Zhang, Y.; Wu, X.; Huang, L.; Li, D.; Fan, W.; Han, G. *J. Am. Chem. Soc.* **2015**, *137*, 5304−5307.

(10) Wu, S.-Q.; Yang, C.-X.; Yan, X.-P. *Adv. Funct. Mater.* **2017**, *27*, 1604992.

(11) Maldiney, T.; Doan, B.-T.; Alloyeau, D.; Bessodes, M.; Scherman, D.; Richard, C. *Adv. Funct. Mater.* **2015**, *25*, 331−338.

(12) Chen, L. J.; Sun, S. K.; Wang, Y.; Yang, C. X.; Wu, S. Q.; Yan, X. P. *ACS Appl. Mater. Interfaces* **2016**, *8*, 32667−32674.

(13) Zheng, B.; Chen, H. B.; Zhao, P. Q.; Pan, H. Z.; Wu, X. L.; Gong, X. Q.; Wang, H. J.; Chang, J. *ACS Appl. Mater. Interfaces* **2016**, *8*, 21603−21611.

(14) Shi, J.; Fu, H.; Sun, X.; Shen, J.; Zhang, H. *J. Mater. Chem. B* **2015**, *3*, 635−641.

(15) Shi, J.; Sun, X.; Li, J.; Man, H.; Shen, J.; Yu, Y.; Zhang, H. *Biomaterials* **2015**, *37*, 260−270.

(16) Wang, T.; Liu, Y.; Wu, C. *Nanoscale Res. Lett.* **2017**, *12*, 66.

(17) Jadhav, N. V.; Vavia, P. R. *AAPS PharmSciTech* **2017**, 1−10.

(18) Zununi Vahed, S.; Salehi, R.; Davaran, S.; Sharifi, S. *Mater. Sci. Eng., C* **2017**, *71*, 1327−1341.

(19) Ying, M.; Zhan, C.; Wang, S.; Yao, B.; Hu, X.; Song, X.; Zhang, M.; Wei, X.; Xiong, Y.; Lu, W. *ACS Appl. Mater. Interfaces* **2016**, *8*, 29977−29985.

(20) Allen, T. M.; Cullis, P. R. *Adv. Drug Delivery Rev.* **2013**, *65*, 36−48.

(21) Lee, J.; Kim, J.; Jeong, M.; Lee, H.; Goh, U.; Kim, H.; Kim, B.; Park, J. H. *Nano Lett.* **2015**, *15*, 2938−2944.

(22) Torchilin, V. P. *Nat. Rev. Drug Discovery* **2005**, *4*, 145−160.

(23) Mo, R.; Jiang, T.; Gu, Z. *Nanomedicine* **2014**, *9*, 1117−1120.

(24) Chithrani, D. B.; Dunne, M.; Stewart, J.; Allen, C.; Jaffray, D. A. *Nanomedicine* **2010**, *6*, 161−169.

(25) Al-Jamal, W. T.; Al-Jamal, K. T.; Cakebread, A.; Halket, J. M.; Kostarelos, K. *Bioconjugate Chem.* **2009**, *20*, 1696−1702.

(26) Meng, H.; Wang, M.; Liu, H.; Liu, X.; Situ, A.; Wu, B.; Ji, Z.; Chang, C. H.; Nel, A. E. *ACS Nano* **2015**, *9*, 3540−3557.

(27) Ravar, F.; Saadat, E.; Gholami, M.; Dehghankelishadi, P.; Mahdavi, M.; Azami, S.; Dorkoosh, F. A. *J. Controlled Release* **2016**, *229*, 10−22.

(28) Nguyen, V. D.; Han, J.; Go, G.; Zhen, J.; Zheng, S.; Le, V. H.; Park, J.-O.; Park, S. *Sens. Actuators, B* **2017**, *240*, 1226−1236.

(29) Molinaro, R.; Corbo, C.; Martinez, J. O.; Taraballi, F.; Evangelopoulos, M.; Minardi, S.; Yazdi, I. K.; Zhao, P.; De Rosa, E.; Sherman, M. B.; De Vita, A.; Toledano Furman, N. E.; Wang, X.; Parodi, A.; Tasciotti, E. *Nat. Mater.* **2016**, *15*, 1037−1046.

DOI: 10.1021/acs.analchem.7b01397
Anal. Chem. 2017, 89, 6936−6939